

Article

Numerical Investigation on Strengthening of Steel Beams for Corrosion Damage or Web Openings Using Carbon Fiber Reinforced Polymer Sheets

Prabin Kumar Silwal¹, Azadeh Parvin^{1,*} and Mohannad Alhusban² 

¹ Department of Civil and Environmental Engineering, The University of Toledo, Toledo, OH 43606, USA; prabin.silwal@rockets.utoledo.edu

² Crawford, Murphy & Tilly, Inc., St. Louis, MO 63102, USA; malhusban@cmtengr.com

* Correspondence: azadeh.parvin@utoledo.edu

Abstract: Fiber-reinforced polymers (FRPs) have been widely used to strengthen steel structures, which could suffer from corrosion or the introduction of web openings, for utilities such as ductwork, plumbing, electrical conduits, and HVAC systems. The present numerical study involves the application of unidirectional carbon FRP (CFRP) sheets to steel I-beams, damaged due to corrosion or web openings, to regain their lost load-carrying capacity. Finite element analysis (FEA) was utilized to develop and validate three beam models against existing experimentally tested specimens. Subsequently, a parametric study was conducted investigating the effect of various corrosion levels and the number of circular web openings on the yield and ultimate load capacities of the beams. The optimum number of CFRP layers needed to strengthen corroded beams was determined and six CFRP strengthening scenarios were adopted to determine the best configurations to retrofit steel beams with openings (SBWOs). The results revealed that corrosion, introduced by thinning the bottom flange, reduced both yield and ultimate load capacities, with a nearly perfect linear reduction in ultimate load for each 2.5% thickness loss. The optimum number of CFRP layers depended on the level of corrosion damage. Furthermore, while maintaining a constant total opening area, beams with a greater number of smaller circular web openings demonstrated higher yield and ultimate load capacities than those with fewer larger openings. Out of the six adopted CFRP strengthening scenarios, three configurations that involved applying CFRP sheets to both flanges and the web effectively restored the strength of SBWOs, when adequate CFRP layers were used.

Keywords: steel beam; strengthening; corrosion; fiber-reinforced polymer; CFRP sheets; web openings; numerical analysis; finite element analysis; ANSYS-MAPDL



Citation: Silwal, P.K.; Parvin, A.; Alhusban, M. Numerical Investigation on Strengthening of Steel Beams for Corrosion Damage or Web Openings Using Carbon Fiber Reinforced Polymer Sheets. *Buildings* **2024**, *14*, 1069. <https://doi.org/10.3390/buildings14041069>

Academic Editors: Grzegorz Ludwik Golewski, Xinghuai Huang and Yeshou Xu

Received: 2 February 2024

Revised: 4 April 2024

Accepted: 9 April 2024

Published: 11 April 2024



Copyright: © 2024 by the authors. Licensee MDPI, Basel, Switzerland. This article is an open access article distributed under the terms and conditions of the Creative Commons Attribution (CC BY) license (<https://creativecommons.org/licenses/by/4.0/>).

1. Introduction

The strengthening and repairing of existing structures are indispensable so that they can function safely, while maintaining serviceability throughout their service life [1]. In steel structures, design errors, environmental conditions, loss of material due to corrosion, sudden unanticipated loadings such as earthquake, etc., warrant strengthening and repair. The conventional strengthening and repair of steel structures involves the addition of steel plates or stiffeners to existing structures. However, it requires heavy tools and equipment to carry steel plates and the welding of steel plates would, ultimately, increase the vulnerability to corrosion and fatigue damages, while also increasing the self-weight of the structure [1,2]. As an alternative to conventional techniques, the use of fiber-reinforced polymers (FRPs) is growing in popularity in the field of structural engineering, along with other areas of civil and mechanical engineering. Being light weight, having a high strength-to-weight ratio, corrosion resistance, durability, and high stiffness are among the desirable properties of FRPs [3,4] that make them an excellent choice for structural strengthening applications.

Many experiments have been conducted to assess the performance of FRP-strengthened steel structures, whose findings point towards their improved performance. It is also observed that the performance of FRP-strengthened structures depends on different parameters such as fiber type, thickness, mechanical properties, fiber orientation, number of layers, etc. [5]. Among the various kinds of available FRP, based on the fiber type, carbon FRP (CFRP) is most widely used because of its higher strength and stiffness. The use of CFRP plates or laminates has been widely studied for the flexural strengthening of steel beams [6,7]. However, the application of CFRP sheets using the wet lay-up technique has not been as popular as laminate plates [8].

Corrosion and delamination in steel structures often lead to the thinning of the flanges in beams and are, therefore, two of the major reasons for the need to strengthen and replace steel structures. Corrosion can gradually weaken steel structures over time, affecting its load-bearing capacity and overall stability. Recent experiments have focused on the durability of FRPs and the FRP–steel bond under different environmental conditions, as well as the effects of corrosion on its durability. An experimental study of CFRP–steel double-strap joints studied under an accelerated corrosion environment showed chances of deterioration in CFRP, resulting in its rupture [9]. Additionally, a study on the influence of corrosion on the bond behavior of CFRP–steel joints showed that some degree of surface irregularity could maximize the bond behavior [10]; however, alternate cycles of dry–wet conditions could cause significant negative impacts on the bond behavior [11].

Additionally, web openings are typically introduced in steel beams to serve a variety of functional and operational demands, such as passage for services (ductwork, plumbing, electrical conduits, etc.), HVAC systems, and other architectural considerations, to achieve specific aesthetic goals. Previous attempts have been made to investigate different types and sizes of web openings, different spacing-to-diameter ratios, the optimal location of openings, different opening ratios and web post widths, and their effects on the overall load-carrying capacity and failure modes of the steel beams [12–16]. The overall load-carrying capacity and stiffness were found to decrease with the increase in the area of each web opening (or increase in the total web opening area), based on those studies. An increase in von Mises stress and shear stress was also observed with an increase in opening area [17]. In this study, the effect of a varying number of web openings of different sizes, with the total web opening area (sum of area of all openings) remaining constant, was investigated. Moreover, the studies that have been made towards the strengthening of steel beams with web openings are limited in number and the strengthening typically involves conventional techniques and materials. Compared to ordinary (homogeneous) beams with web openings, an increase in strength was observed in hybrid beams (made up of beams with web and flange plates of different strengths) [18]. Additionally, a study on strengthening techniques involving the use of steel stiffeners around web openings [19] and the application of steel flange cover plates at the flange bottom [20] demonstrated their effectiveness. The use of CFRP plates to strengthen simply supported steel I-beams with rectangular web openings was also studied experimentally and improvements in load-carrying capacity and stiffness were observed [21]. However, rectangular openings in steel I-beams may introduce higher stress concentrations around their perimeter, particularly near the corners, compared to circular ones, which could potentially limit the FRP's efficacy. In addition, given the complex behavior of steel I-beams with openings, which introduces challenges for reinforcement, the use of FRP sheets emerges as a more feasible option compared to FRP plates. Therefore, the use of FRP sheets in steel I-beams with circular instead of rectangular web openings and the optimization of strengthening layouts need to be investigated.

Based on the existing literature, studies on the efficacy of CFRP sheets on strengthening steel I-beams, damaged due to corrosion and cut-out web openings, are limited. Therefore, the present FEA study investigates the effect of corrosion on the flexural strength of as-built steel beams and the optimum number of CFRP layers required in restoring their strength. This study further examines the strengthening of steel beams with web openings

introduced at the flexure-dominated region of the beam, near the mid-span, using CFRP sheets. Specifically, six different strengthening layouts, each considering various numbers of CFRP layers, were adopted to identify the optimal configurations.

2. Description of the Experiment Used for the Validation of FE Models

This section describes the experimental study by Bastani et al. [8] used in the validation of the developed FE models. Three FE models have been validated with their respective experimental tests. The experiments were performed on simply supported steel I-beams under four-point bending loading. The load was applied using a simply supported spreader beam with a span of 500 mm and transferred to the specimen using two steel plates [8]. The effective and total span lengths of the specimens were 1500 mm and 2000 mm, respectively. The first developed FE model was validated against the tested undamaged un-strengthened control steel beam (CV-00), as shown in Figure 1. The second FE beam model was developed based on specimen CD-20, in which the bottom flange was thinned out to simulate corrosion effects. The maximum thinning was 20% of the thickness of the bottom flange. The specimen was thinned out in a circular profile, such that the total length of damage was 100 mm, as shown in Figure 2. Lastly, the third tested beam taken for validation was RB-20-2L (Figure 3), representing the rehabilitated version of the CD-20 beam by using two layers of CFRP sheets at the bottom face of the bottom flange. Unidirectional CFRP sheets were oriented along the longitudinal axis of the beam. The CFRP sheets were soaked in epoxy resin and then attached to the bottom flange using a wet lay-up method. CFRP cross-wraps were used to prevent debonding between steel and longitudinal CFRP sheets. The material properties of steel and CFRP sheets used in the development of FE models are presented in Table 1.

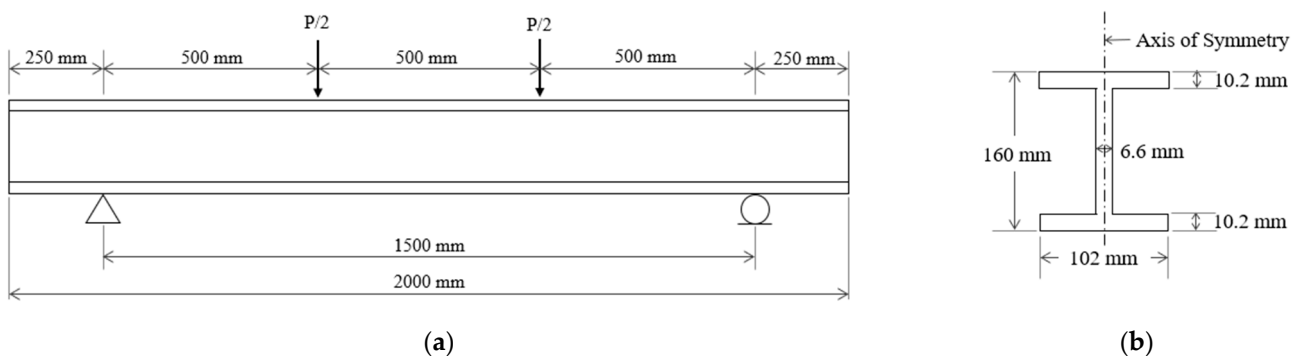


Figure 1. Beam CV-00 details and dimensions: (a) elevation; (b) cross section. (Data from Bastani et al., 2019 [8]).

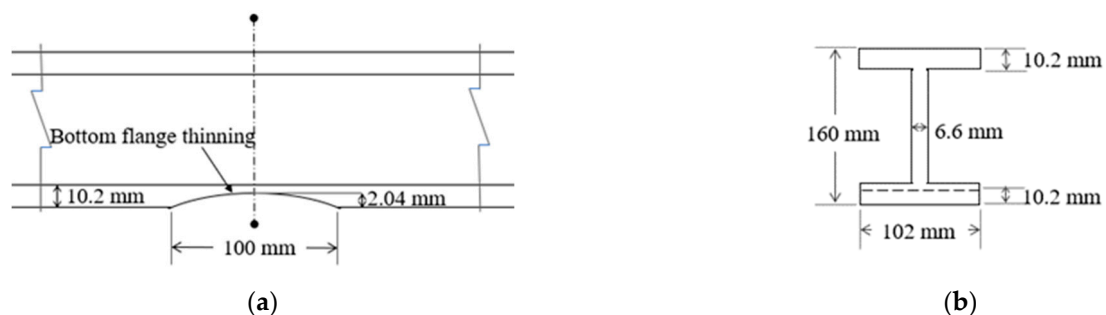


Figure 2. Beam CD-20 with 20% thinning: (a) elevation; (b) cross section. (Data from Bastani et al., 2019 [8]).

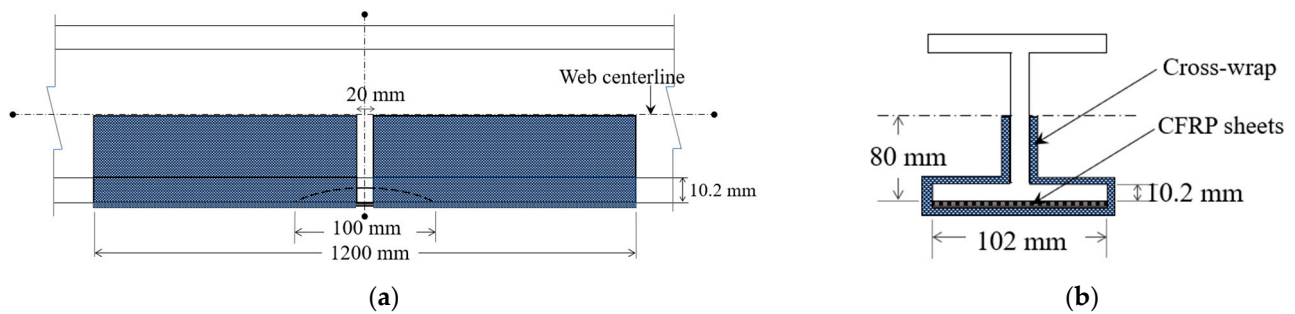


Figure 3. CFRP-strengthened beam (RB-20-2L): (a) elevation; (b) cross section. (Data from Bastani et al., 2019 [8]).

Table 1. Material properties of steel and CFRP sheets (Data from Bastani et al., 2019 [8]).

Material	Mechanical Properties	Symbol	Unit	Value
Steel	Yield stress	f_y	MPa	379
	Ultimate stress	f_u	MPa	484
	Yield strain	ϵ_y	%	0.2
	Ultimate strain	ϵ_u	%	35
	Elastic Modulus	E	GPa	205
	Poisson's ratio	μ	-	0.3
CFRP	Sheet thickness	-	mm	0.26
	Tensile strength in longitudinal direction (0°)	-	MPa	1780
	Tensile modulus in longitudinal direction (0°)	-	GPa	152
	Tensile elongation in longitudinal direction (90°)	-	%	1.75
	Tensile strength in transverse direction (90°)	-	MPa	60
	Tensile modulus in transverse direction (90°)	-	GPa	9
	Tensile elongation in transverse direction (90°)	-	%	0.5
	In-plane shear strength	-	MPa	100
	In-plane shear modulus	-	GPa	12

3. Finite Element Modeling Procedure

The numerical models were developed using a nonlinear FEA software program, ANSYS 2020 R2, which was used to model steel beams. FE models were developed in accordance with the geometry, material properties, loading, and boundary conditions of the experimental setup [8]. The steel beams, loading and supporting plates, and CFRP sheets were modeled using element type 'SOLID185', which is an eight-node 3D element having plasticity, hyperelasticity, stress stiffening, creep, large deflection, and large strain capabilities [22]. Both the elastic and plastic properties were assigned for steel.

To define linear elasticity, the modulus of elastic moduli and Poisson's ratio were assigned. Strain-hardening in steel after yielding was considered using ANSYS's multilinear-isotropic material model in which the yield and ultimate stress and strain values were assigned (Table 1). The resulting stress–strain curve for the steel exhibits a bilinear behavior. For the steel plates, only linear elastic behavior was assumed, with the modulus of elasticity 'E' and Poisson's ratio of the steel being assigned. On the other hand, CFRP sheets were modeled as a linear–elastic material up to its rupture using ANSYS's linear–orthotropic material model. The material properties of CFRP sheets are provided in Table 1. To define the linear–orthotropic material model in ANSYS, only the elastic moduli in three (x , y , and z) directions and Poisson's ratios and shear moduli in all three (xy , yz , and xz) planes were defined. The elastic modulus in the three directions (E_x , E_y , and E_z) were assigned as 152, 9, and 9 GPa, respectively. Poisson's ratios (μ_{xy} , μ_{yz} , and μ_{xz}) were all input as 0.3 and the shear moduli in all three planes (G_{xy} , G_{yz} , and G_{xz}) was assigned as 12 GPa. The tensile and shear strength of CFRP and the tensile elongations were used to identify when the failure is reached in the models.

CFRP layers were modeled as distinct solid layers and a perfect bond at the interlaminar interface between the layers was ensured by merging the coincident nodes. In addition, since debonding did not occur in test specimens, steel and CFRP sheets were connected in FE models, assuming a perfect bond by merging only the coincident nodes between the two surfaces, as in the experiment. This simplified method yields similar outcomes to the bonded surface-to-surface contact method that assumes no relative motion or slippage between the two materials at their interface. Similarly, the bond behavior between the steel beam and loading and supporting plates was assumed to be perfect.

The use of finer mesh improves the convergence of FE results and yields more accurate predictions [8]. Based on a mesh sensitivity analysis, the largest element size selected was 5 mm. When compared with the experimental results, the yield, ultimate loads, and failure mode of the FE models agreed well with experimental results. Additionally, the CFRP sheet used in this test was very thin (0.26 mm thickness). Therefore, the selection of 5 mm avoids an element aspect ratio exceeding ANSYS's warning limit of 20, to eliminate the distortion of irregular or thin elements.

Due to symmetry (refer to Figure 1b), only the symmetrical half of the beam was modeled. The developed FE model of the control beam (CV-00) is shown in Figure 4a. The experiment was carried out using simply supported boundary conditions. Therefore, restraints were assigned at the support locations in the model. To model a hinged support, restraints were assigned for all three directions, X , Y , and Z , and to model roller support, restraints were assigned only in the Y and Z directions for the line of nodes located at the location of supports. Likewise, the nodes along the plane of symmetry were constrained using roller supports in the perpendicular direction (Z), as shown in Figure 4b.

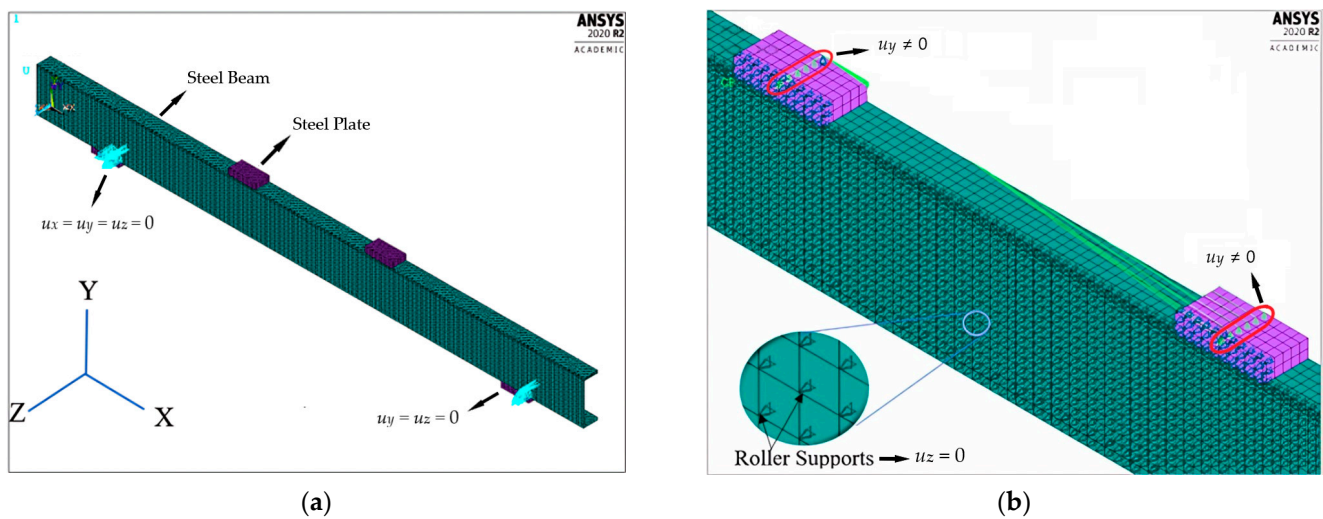


Figure 4. (a) FE model of control beam (CV-00); (b) roller supports perpendicular to axis of symmetry.

In the experimental study [8], the loading of the beams was carried out monotonically, using the displacement control method. The loads were applied to the steel plates at the top flange of the beams to avoid any stress concentration and to ensure a smooth load transfer between the nodes of the plates and the beam. To achieve convergence and to avoid premature failure of the beams, a displacement-controlled analysis was implemented by gradually applying a vertical displacement on the top loading plates. To ensure the same displacement would be applied at the corresponding loading locations, the nodes at the location of application of point loads were tied together in the Y direction using the “coupling” feature of the ANSYS preprocessor, so that all the coupled nodes would displace vertically by the same amount.

4. Validation of Developed FE Beam Models

The developed finite element models were validated against their experimental counterparts. The models were validated both at the yield and failure stages. Figures 5–7 show load versus mid-span displacement curves of the validated beam models. The FEA and experimental results are compared to each other and are in good agreement, with less than a 4% difference, as shown in Table 2.

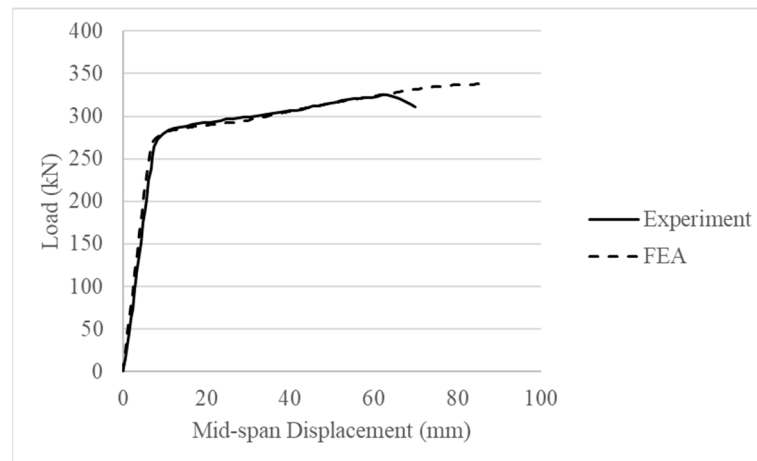


Figure 5. Load versus mid-span displacement curve for CV-00.

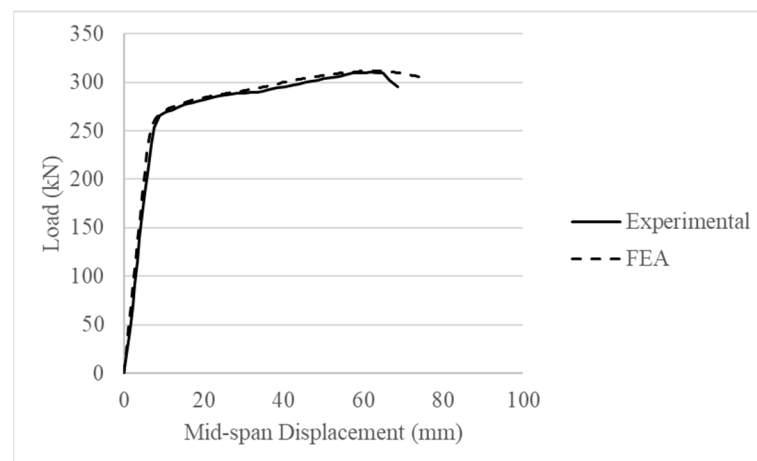


Figure 6. Load versus mid-span displacement curve for CD-20.

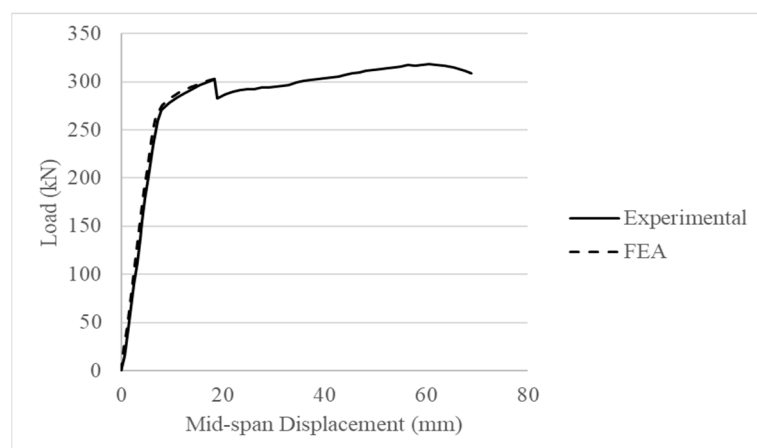


Figure 7. Load versus mid-span displacement curve for RB-20-2L.

Table 2. Comparison of experimental and FEA results.

Beam ID	Yield Load (kN)			Ultimate Load (kN)			CFRP Rupture Load (kN)		
	Experiment	FEA	Difference (%)	Experiment	FEA	Difference (%)	Experiment	FEA	Difference (%)
CV-00	273	272	0.4	325	338	4	-	-	-
CD-20	255	256	0.4	312	312	0	-	-	-
RB-20-2L	270	271	0.4	-	-	-	303	304	0.3

As indicated in the previous section, CV-00 is the control (undamaged) beam and '00' represents no (0%) damage; CD-20 is the control damaged beam and '20' represents 20% damage (maximum 20% thickness loss of the bottom flange); RB-20-2L represents the rehabilitated beam, which had a maximum 20% thickness loss with 2 layers of CFRP sheets [8].

FE Beam Models Failure Behavior

The yield load was obtained in the experiment [8] when the beam specimen reached the yield strain value of 0.2%, which was recorded using the strain gauge mounted at the mid-span of bottom flange. In the developed FE models, the beam was considered to have yielded after the strain value of 0.002 was reached at the flange gauge location in the experiment. The corresponding load at the same time step was the yield load of the FE beam models. The ultimate load in the experimental study was taken to be the maximum load that the beam could carry before the load started to drop as the applied displacement increased. In the cases of the developed FE models of the control undamaged beam, CV-00, and the control damaged beam, CD-20, the load versus mid-span deflection data points were extracted from ANSYS and plotted using a spreadsheet. The load was observed to reach a certain maximum value (the ultimate load) and was then gradually decreased, as the mid-span displacement increased. Likewise, the observed load versus mid-span deflection of the CFRP-strengthened beam, RB-20-2L, in the experiment could be divided into five segments [8]. Among those segments, the sudden vertical drop is of interest and is caused by the rupture of CFRP sheets. This sudden vertical drop is due to the brittle nature of CFRP sheets, whose rupture is abrupt and without warning [8]. After the rupture of the CFRP sheets, the load versus deflection curve follows a similar trend to that of the un-strengthened beam [8]. In the developed FE model of the strengthened beam, RB-20-2L, the CFRP rupture point was regarded as the failure point and only the behavior up to the CFRP rupture point was validated, as shown in Figure 7. Modeling the behavior of FRP-strengthened steel beams after a load drop in ANSYS is highly challenging due to the abrupt change in load distribution and the potential for localized damage or failure. The CFRP rupture point was identified in the FEA when the maximum stress in the CFRP sheet reached its tensile strength of 1780 MPa.

5. Parametric Study Results

After the validation of FE models, various scenarios such as corrosion damage and web opening cutout were considered, to study the behavior of steel beams and the efficacy of CFRP sheets in restoring the load capacities of the altered beams. To strengthen the beams subjected to corrosion damage, CFRP sheets were applied to their bottom flanges, whereas six CFRP strengthening configurations were studied in detail to determine the efficient strengthening configuration to strengthen steel beams with web openings (SBWOs). The subsequent section presents the parametric study carried out on the validated FE model of the control beam, 'CV00', which is the undamaged steel beam. Other beams, 'CD-20' and 'RB-20-2L', were validated to enhance the accuracy of developed FE models.

5.1. Effect of Corrosion and CFRP Strengthening

The effect of corrosion in steel beams was incorporated in the FE model by reducing the thickness of the bottom flange. The study was conducted in five distinct levels of corrosion damage, i.e., 2.5%, 5%, 10%, 15%, and 20% thinning of the bottom flange, corresponding to 0.26 mm, 0.52 mm, 1.04 mm, 1.56 mm, and 2.08 mm thinning, respectively. The thinning was introduced to 80% of the beam effective span (refer to Figure 8) to emulate non-localized corrosion cases and maximize the effects due to thinning.

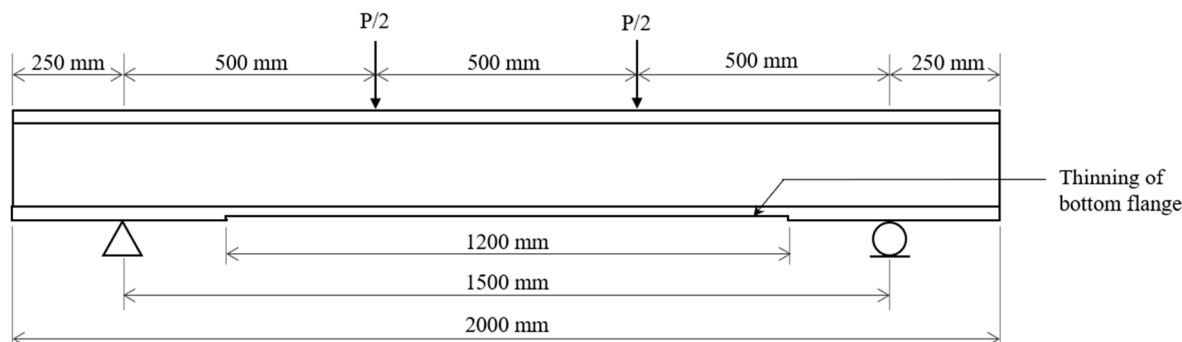


Figure 8. Beam subjected to thinning at the bottom flange.

The FE beam models are named to indicate the damage level and number of layers of CFRP sheets used for rehabilitation. The model ID is divided into two parts, using a dashed line if the model is a strengthened beam. The first and second parts specify the type of damage and number of layers of CFRP sheets, respectively. In the first part, the letter 'D' indicates that the beam is damaged. The number following the letter 'D' indicates the level of corrosion damage. In the second part, the first letter 'R' indicates that the beam has been rehabilitated and the remaining letters 'nL' refers to the number of layers of CFRP sheets used for strengthening. The beams without rehabilitation do not have the second part in their IDs.

The effect of thickness loss of the bottom flange on the yield and ultimate load of the beam is tabulated in Table 3. The load versus mid-span displacement diagram is shown in Figure 9. As the level of bottom flange damage (thickness loss) increased, the reduction in the yield and the ultimate load also increased. Both the reduction in yield and ultimate loads followed a linear trend, as shown in Figure 10.

Table 3. Effect of bottom flange thinning.

Beam ID	Yield Load (kN)	Reduction in Yield Load Capacity (%)	Ultimate Load (kN)	Reduction in Ultimate Load Capacity (%)
D2.5	272	0	333	1.5
D5	268	1.5	328	3.0
D10	261	4.0	317	6.2
D15	256	5.9	307	9.2
D20	249	8.5	296	12.4

Note: reductions in the load capacities are obtained by comparing the undamaged beam (CV-00) to the damaged ones.

To strengthen the damaged beams, successive layers of CFRP sheets were attached to the bottom face of the bottom flange, covering the damaged (thinned out) area, as shown in Figure 11. The unidirectional CFRP sheets were oriented along the longitudinal axis of the beam.

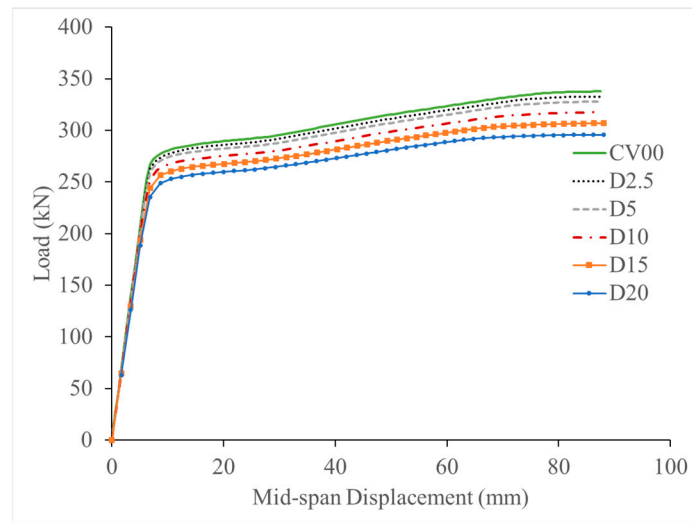


Figure 9. Load versus mid-span displacement behavior of corroded steel beams.

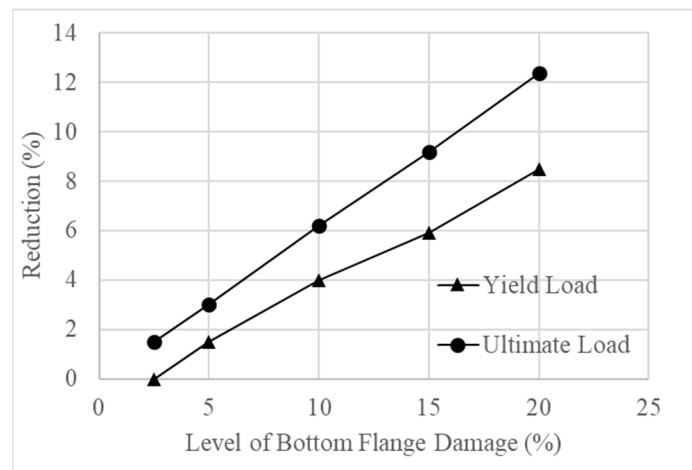


Figure 10. Reduction in load capacities of corroded steel beams.

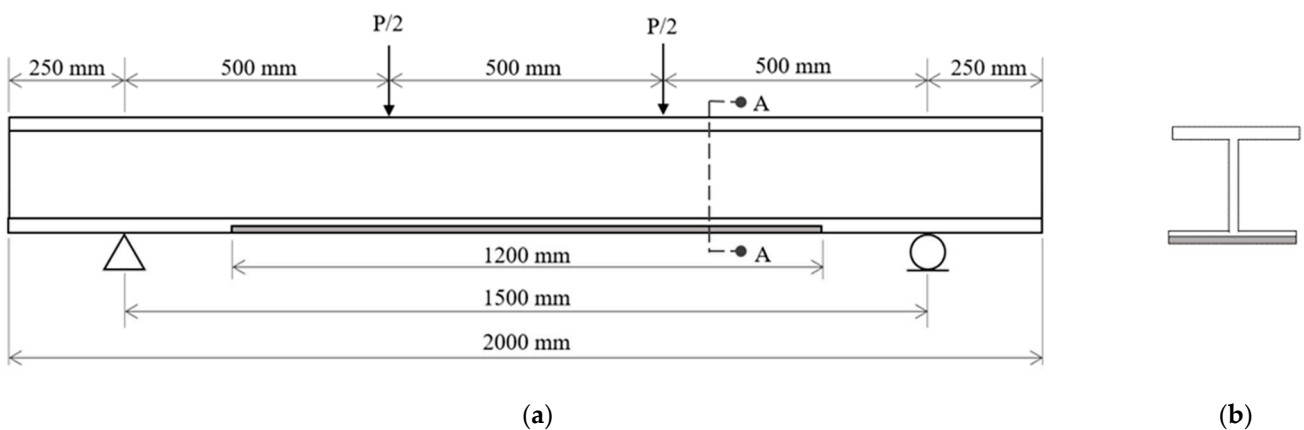


Figure 11. CFRP strengthening in beams subjected to thinning of bottom flange: (a) elevation; (b) section A-A.

Seventeen FE models were developed for different levels of corrosion damage. The initial number of layers of CFRP sheets for each level of corrosion damage was based on the number of layers required by the previous level of corrosion damage and the layers were added successively until both the target yield and ultimate capacities were reached. The

observed yield and the failure loads for each FE model are shown in Table 4. The failure load was reached when the CFRP sheets began to rupture. Debonding was prevented in the experiment using cross-wraps [8]. Therefore, the debonding of the CFRP sheets was not allowed in the FE models.

Table 4. Yield and failure loads after CFRP strengthening in FE beam models subjected to thinning of the bottom flange.

Beam ID	Yield Load (kN)		Failure Load (kN)	
	Target Value	FEA Results	Target Value	FEA Results
D2.5-R1L	273	275	325	302
D2.5-R2L		279		319
D2.5-R3L		282		336
D5-R1L	273	272	325	299
D5-R2L		276		316
D5-R3L		279		331
D10-R3L	273	273	325	325
D10-R4L		276		342
D15-R3L	273	266	325	317
D15-R4L		270		333
D15-R5L		273		350
D15-R6L		276		365
D20-R4L	273	251	325	325
D20-R5L		267		342
D20-R6L		270		357
D20-R7L		273		373
D20-R8L		276		387

The study focused on the optimum number of layers of CFRP sheets needed to restore the yield and the ultimate load capacities of the damaged beam to the original undamaged state (to that of CV-00). By doing so, an improvement in the serviceability requirements in terms of reduction in the mid-span deflection due to the application of CFRP was also observed.

For the beam with damage level of 2.5% (D2.5 beam), one layer of CFRP strengthening would be sufficient to restore the yield load capacity; whereas, three layers were required to restore the ultimate load capacity to that of the undamaged control beam 'CV00' (Table 4). Similarly, for the 'D5' beam, two layers of CFRP sheets were sufficient to restore the yield load capacity; however, three layers were needed to restore the ultimate load capacity. For the 'D10' beam, three layers of CFRP sheets were just sufficient to reach the yield and ultimate load capacities and four layers were needed to exceed those capacities. For the 'D15' beam, four layers were sufficient to restore the ultimate load capacity, whereas six layers were needed to exceed the target yield load capacity. For the 'D20' beam, five layers were needed to exceed the target ultimate load. However, eight layers were needed to exceed the target yield load.

It is also observed that the failure load of the 'D2.5-R1L', 'D2.5-R2L', 'D5-R1L', and 'D5-R2L' strengthened beam models (Table 4), which correspond to CFRP rupture, is less than the ultimate load of the damaged beams 'D2.5' and 'D5' (Table 3). It may give the impression that the strengthening worked to the opposite effect. However, the load versus mid-span deflection curves of these beams shows a considerable improvement in the stiffness of the inelastic regime and the reduction in the mid-span deflection, due to strengthening. Consequently, the lower number of CFRP sheet layers in these beams was subjected to higher levels of stresses, due to which they ruptured at lower load levels.

Figure 12 shows the load versus mid-span deflection curves for all FE beam models. It is observed that a higher number of CFRP layers resulted in a reduced mid-span deflection

and improved stiffness and the adequate number of layers of CFRP sheets that depends upon the level of damage, as presented in Table 4, could fully restore the yield and ultimate load capacities of corroded beams to the level of the undamaged beam.

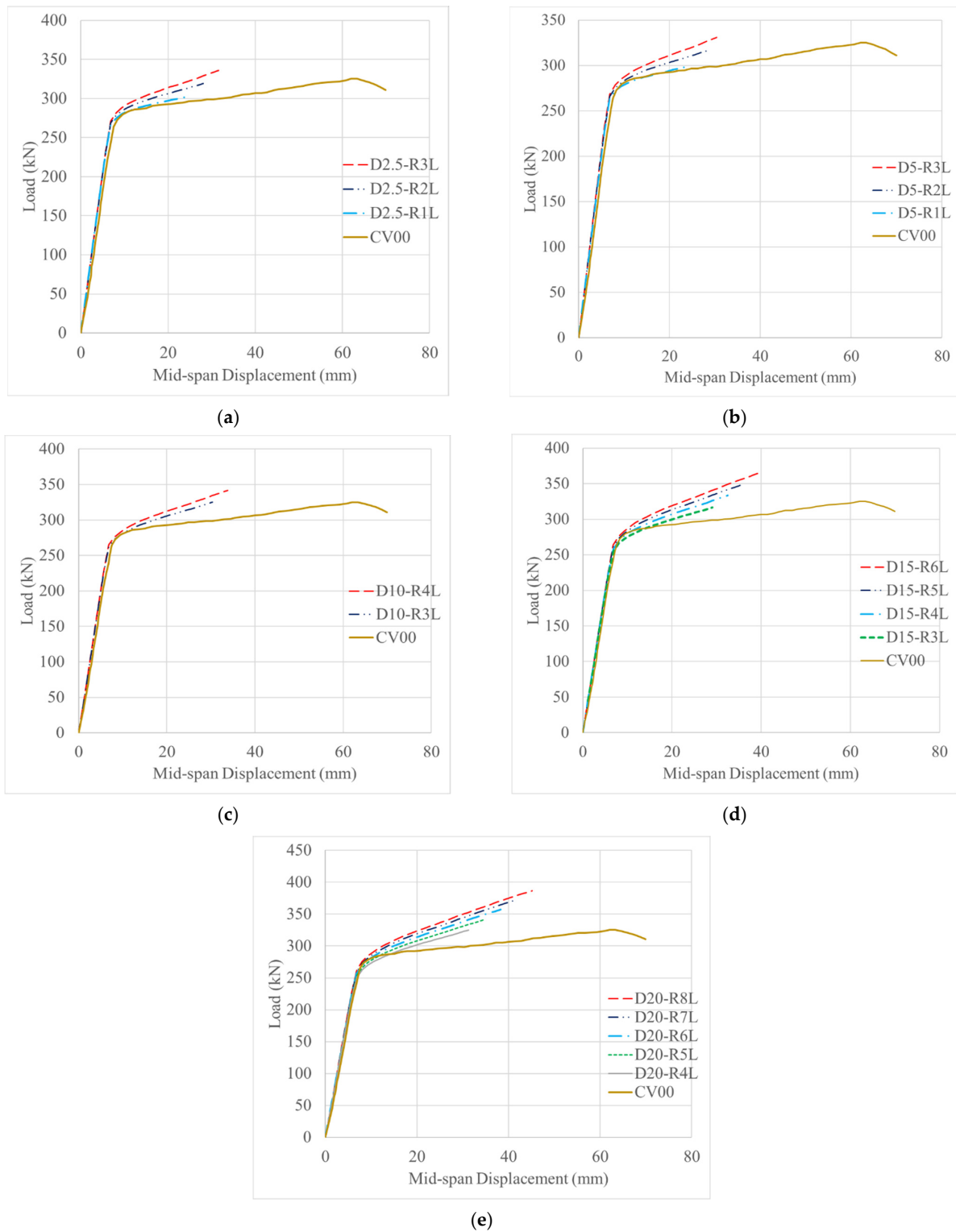


Figure 12. Load versus mid-span displacement behavior of undamaged (CV-00) and strengthened beams with: (a) 2.5% damage; (b) 5% damage; (c) 10% damage; (d) 15% damage; and (e) 20% damage.

5.2. Effect of Web Openings

Past studies [12,13,16] have shown that the performance of steel beams with circular web openings is superior to that of other opening shapes. For the same opening area, steel beams with circular web openings had a higher ultimate load capacity and lower stress concentrations around their edges. Therefore, circular openings were considered in the present study. Since the bending stresses are at a maximum at the extremities and the shear stress is the highest at the neutral axis of the cross-section, the flanges and the web should be able to resist high bending stresses and high shear, respectively. Therefore, it is prudent to provide openings in the web (where shear stress is at a maximum) in the regions of low shear forces. One study [14] concluded that the openings are to be provided in the bending predominant region instead of in the shear predominant region, and the optimal location of web openings is the middle two-thirds of the beam's span, which is a bending predominant region.

Under the four-point bending load, the middle-third span of the beam is subjected to pure bending and there is no shear force. Therefore, openings were introduced at this location of the beam, as shown in Figure 13. Design guidelines across the globe have provisions and limits on the dimension and location of openings, spacing between openings, etc. Therefore, an offset from point load 'C' and clear spacing between openings 'S', in this study, were chosen based on the SCI P355 [23], which suggests generalized design methods for discrete or closely spaced web openings.

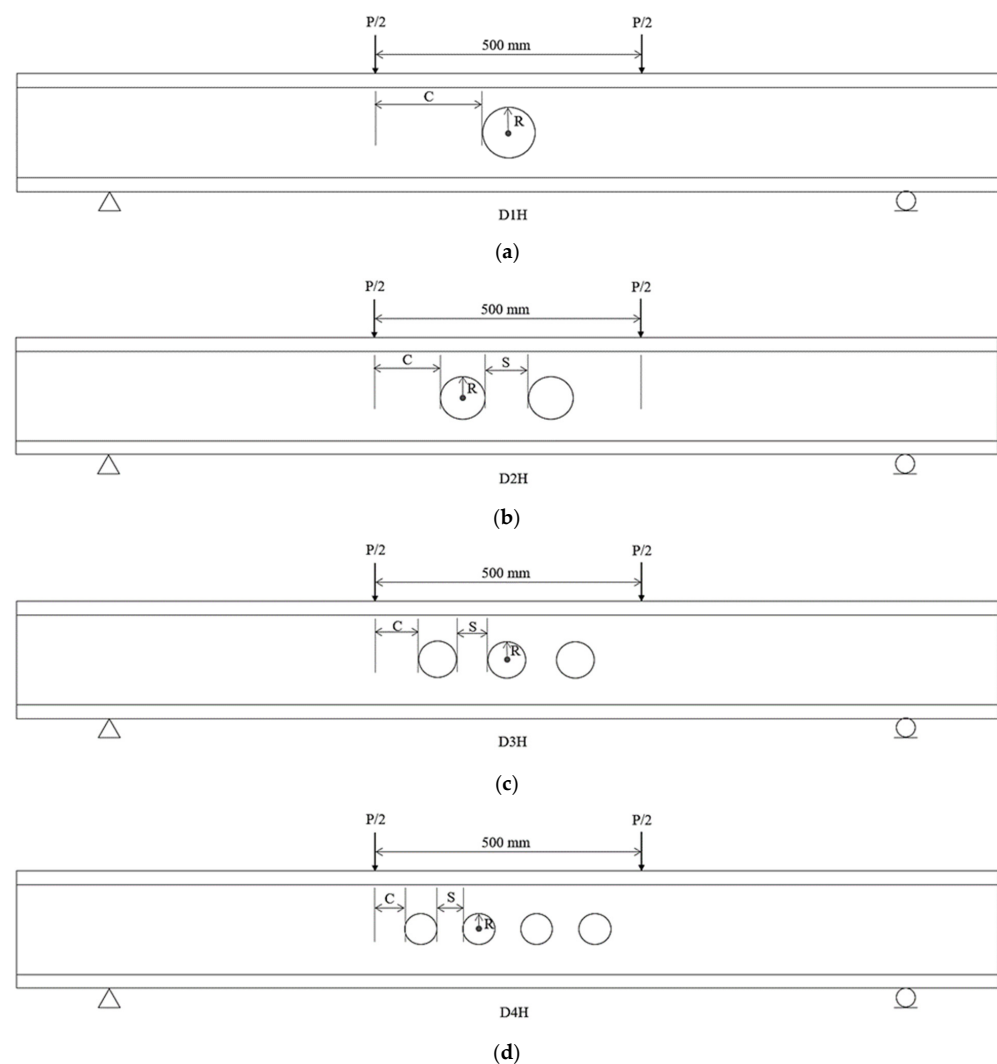


Figure 13. Steel beams with circular web openings (SBWOs) with: (a) one opening; (b) two openings; (c) three openings; and (d) four openings.

In total, four FE beam models with different sets of web openings were studied, with the number of openings ranging from one to four, as shown in Figure 13. The total area of openings in all the beams was kept nearly constant. The details and dimensions of the beam models are described in Table 5.

Table 5. Details and dimensions of web openings shown in Figure 13.

Beam ID	'C' (mm)	'S' (mm)	'R' (mm)	'N'	'Ae' (mm ²)	'A' (mm ²)	Area Ratio	Opening Ratio
D1H	193.5	-	56.5	1	10029	10029	1.000	0.71
D2H	80	180	40	2	5027	10053	1.002	0.50
D3H	80	71	33	3	3421	10264	1.023	0.41
D4H	80.5	37	28.5	4	2552	10207	1.018	0.36

Note: 'C' = offset from point load; 'S' = clear spacing between openings; 'R' = radius of each opening; 'N' = number of openings; 'Ae' = area of each opening; 'A' = total area of openings; 'Area Ratio' = Total area of openings of each model (A) divided by total opening's area of D1H; and 'Opening Ratio' = depth (diameter) of opening divided by depth of beam.

The nomenclature of the beams is such that the first character 'D' indicates the damage induced by the web opening and the remaining characters, 'nH', indicate 'n' number of circular web openings or holes in the beam. The load versus mid-span deflection curves for the FE models are shown in Figure 14. The maximum load attained is the ultimate failure load, after which, the load started to drop upon further increase in applied displacement.

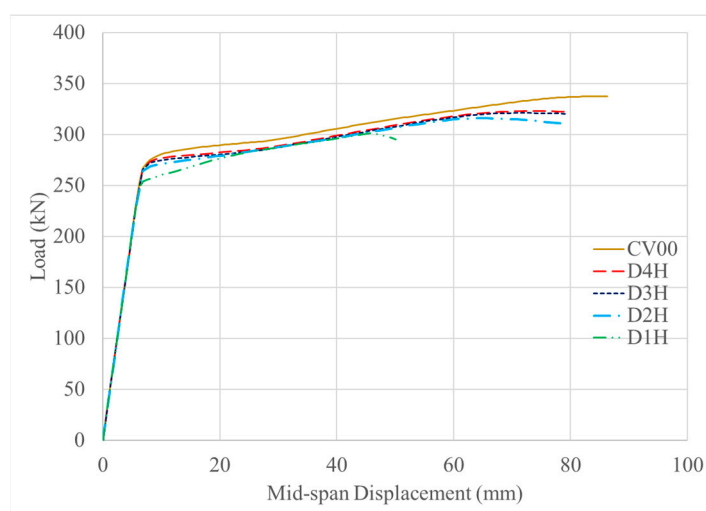


Figure 14. Load versus mid-span displacement behavior of SBWOs.

To obtain the reduction in the load capacities, as tabulated in Table 6, the beam models with openings (D1H, D2H, D3H, and D4H) were compared to that of the undamaged beam (CV-00).

Table 6. Effects of introduction of web openings.

Beam ID	Reduction in Yield Load Capacity (%)	Reduction in Ultimate Load Capacity (%)
D1H	6.6	10.9
D2H	1.1	6.5
D3H	0	5
D4H	0	4.4

For SBWOs with an opening ratio <0.5 (D3H and D4H), the maximum reduction in ultimate load capacity was 5% and there was no effect on the yield load capacity. However, for model D1H with an opening ratio >0.5 , the reduction in the ultimate and yield load

capacities was the highest. In general, it was observed that beams with a higher number of circular web openings and smaller sizes had higher load capacities, as compared to those with a smaller number of bigger openings, if the total area of the openings was kept constant.

Based on previous studies [15,21], commonly observed global failure modes in SBWOs are flexural, Vierendeel mechanism, and web-post buckling. The flexural failure mode, also known as the flexural mechanism, is predominant in the region with high bending moments, as it could lead to yielding of T-regions below and above the web openings and the consequent formation of plastic hinges. The Vierendeel mechanism is a failure due to the formation of plastic hinges at the corners of the T-regions above and below the openings, causing them to deform. It is observed in the region with high shear forces. Web-post buckling generally occurs when the openings are closely spaced without sufficient clear spacing between the adjacent openings. Since the openings were introduced in the middle-third of the beam span, where it was subjected to high bending moments and low shear, the flexural failure mode was anticipated in all four beam models, D1H, D2H, D3H, and D4H. The stress diagrams of the beam models at the ultimate load are shown in Figure 15. The stress contour shows that both the top and bottom Ts at the opening locations had yielded as the average stress in those T-regions were higher than the yield stress. Therefore, it was confirmed that the governing mode of failure was the flexural failure mode.

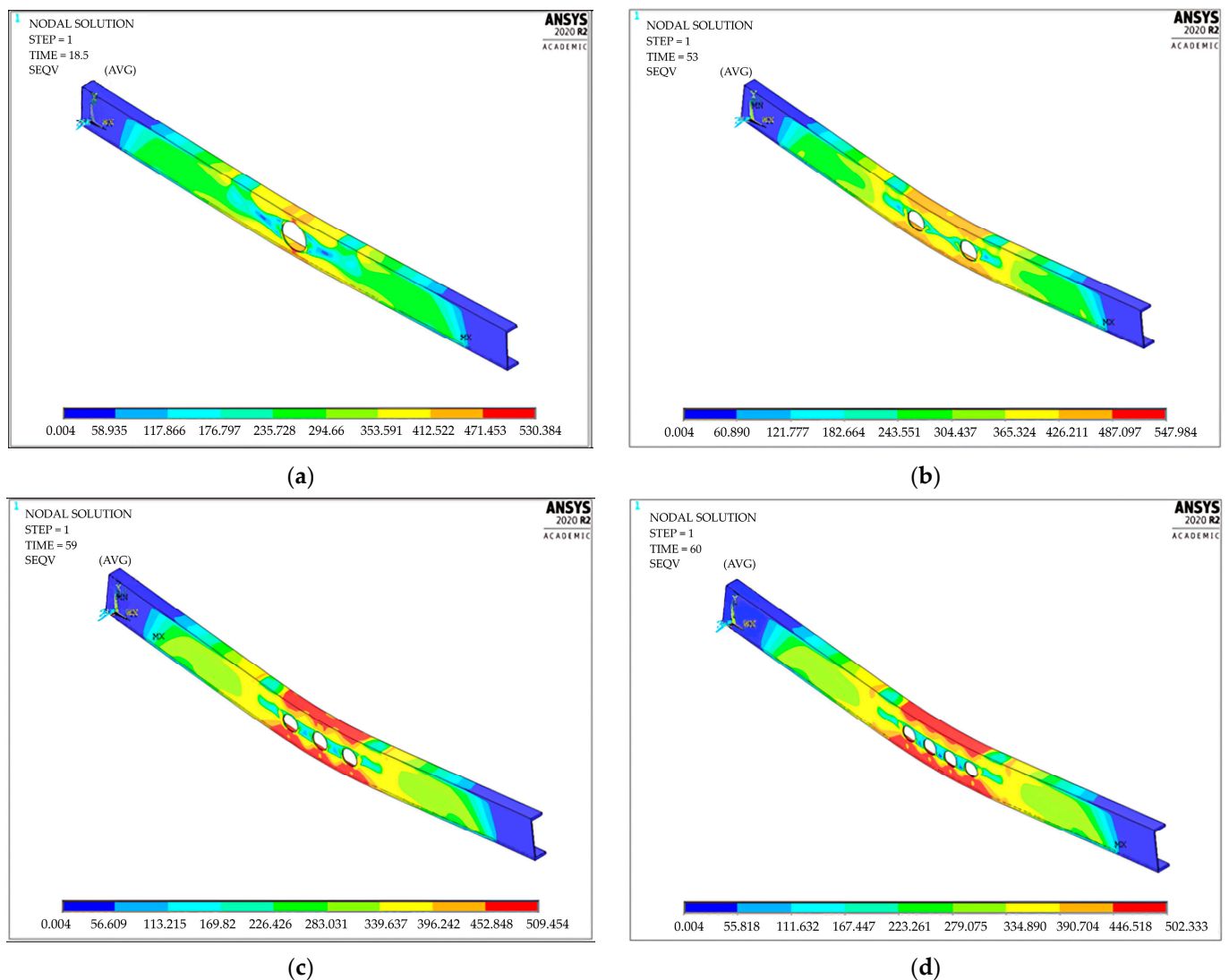


Figure 15. von Mises stress distribution at ultimate stages for SBWOs: (a) D1H; (b) D2H; (c) D3H; and (d) D4H.

The maximum ultimate load reduction of 10.9% (refer to Table 6) occurred in model D1H, which had an opening ratio of 0.71 (refer to Table 5). The area of the web opening was equal to 4.8% of the total area of the web, along the span of 1500 mm.

Most available design guidelines, including SCI P355 [23], allow for a maximum opening ratio of 0.8. Therefore, another model—D1H*, with maximum permissible opening ratio of 0.8—was developed. Figure 16 shows the dimensions and location of the opening. The load versus mid-span deflection curve for D1H* is shown in Figure 17, which is compared against the steel beam without an opening (CV00).

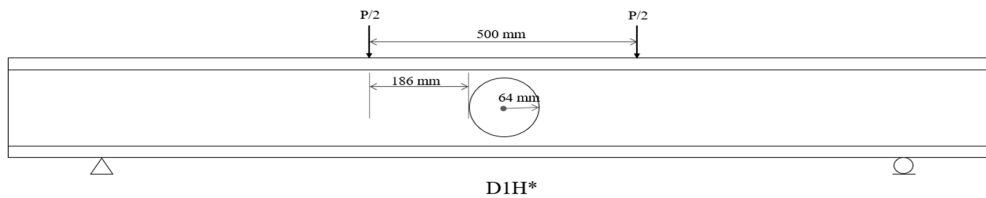


Figure 16. Steel beam with maximum opening ratio.

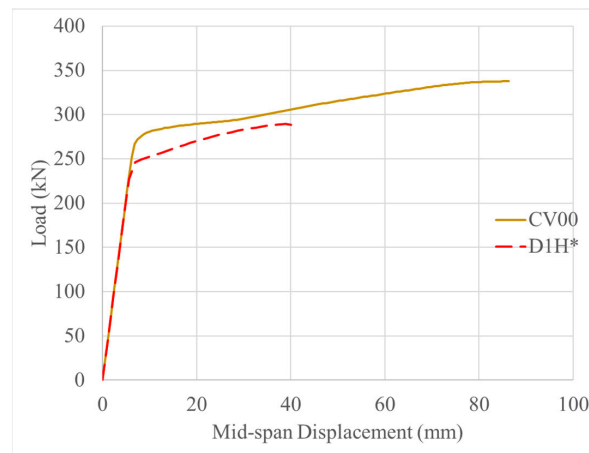


Figure 17. Load versus mid-span deflection curve of beam model D1H*.

Compared to the control undamaged beam (CV00), reductions of 9.6% and 14.5% in the yield and ultimate load capacities were observed for D1H*. The stress distribution diagram of D1H* at the ultimate stage is shown in Figure 18. The stress on the top and bottom Ts exceeded yield stress and were close to ultimate strength of steel. Therefore, the governing failure mode for D1H* was the flexural mechanism.

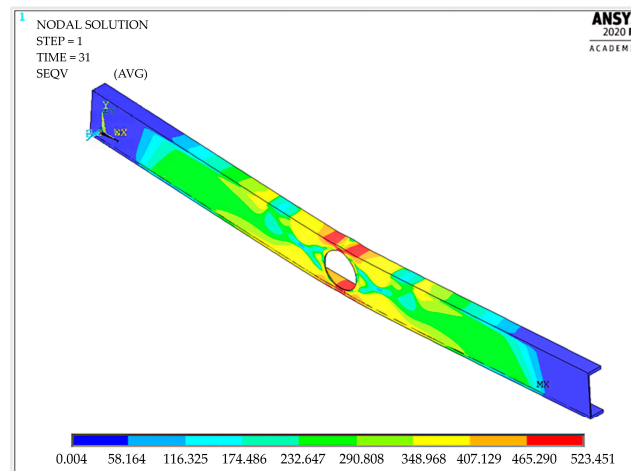


Figure 18. von Mises stress distribution of D1H* at ultimate load stage.

5.3. CFRP Strengthening of Steel Beams with Openings

The use of FRP is generally more efficient in strengthening weak beams compared to strong beams. Therefore, the beam model D1H*, with the highest loss of load capacity due to opening, was selected for CFRP strengthening. Six different CFRP strengthening configurations (schemes) were examined. The mode of application of CFRP sheets for each scheme is shown in Figure 19, where the shaded blocks represent CFRP sheets. The first strengthening layout was selected based on the failure of the D1H* beam, which failed in the flexural mechanism, with high stresses observed at the bottom and top flanges. Consequently, each strengthening arrangement was selected based on the predicted failure or limitation of the previous configuration. The aim of adopting various strengthening arrangements is to determine the most efficient strengthening configuration to strengthen steel beams with web openings. The specifics of each strengthening scenario are discussed in detail in the subsequent paragraphs. It is noted that all CFRP sheets were oriented along the longitudinal axis of the beam, including the ones applied to the beam's web.

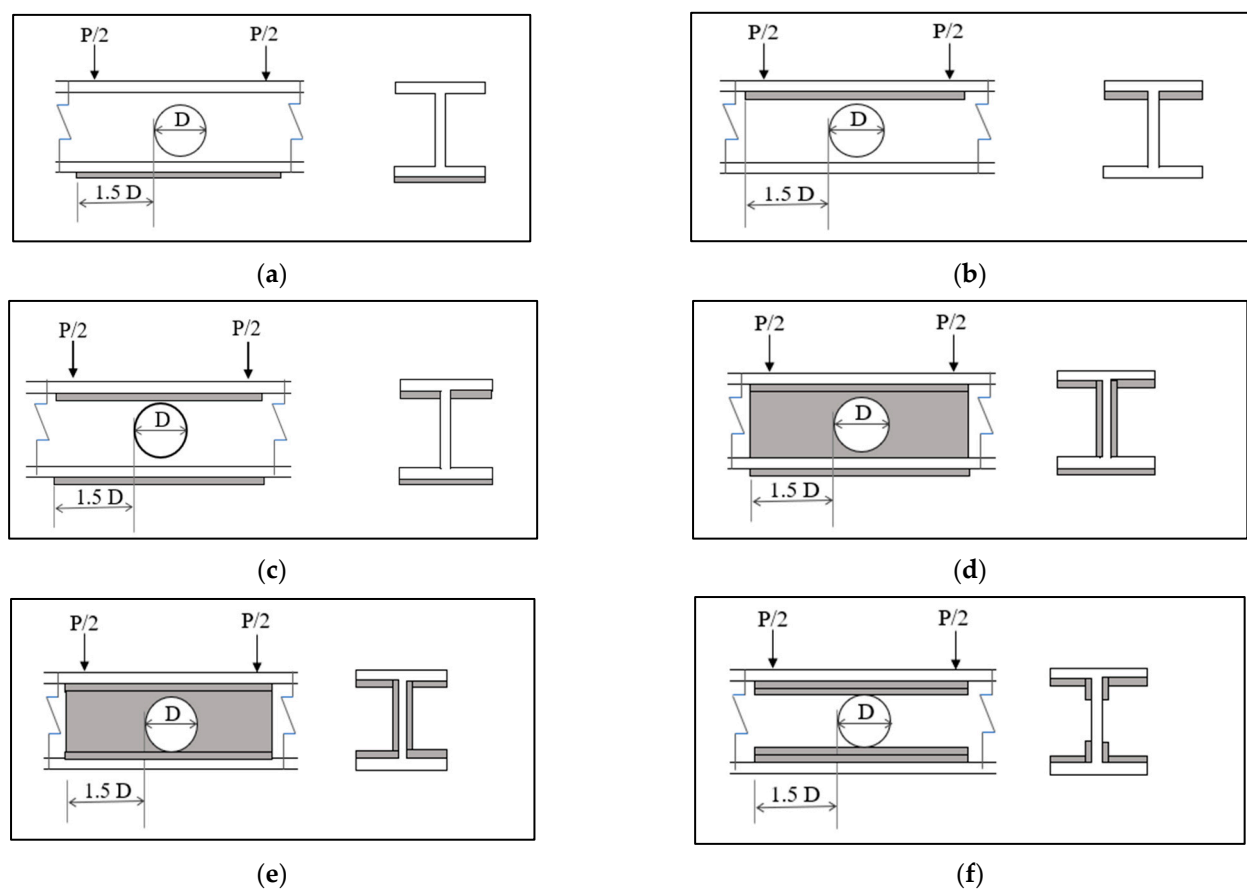


Figure 19. CFRP-strengthening of SBWOs: (a) Scheme-I; (b) Scheme-II; (c) Scheme-III; (d) Scheme-IV; (e) Scheme-V; and (f) Scheme-VI.

The first strengthening strategy, ‘Scheme-I’ was based on the application of CFRP sheets on the bottom of the beam’s bottom flange, as shown in Figure 19a. The total length of the CFRP sheet was taken as four times the size of the opening. Therefore, the CFRP sheets were extended beyond the edge of the opening, by 1.5 times the opening size, from both sides, as shown in Figure 19. The selection of this length was based on a previous study [24] on the optimal length of CFRP to strengthen steel beams with openings. The analysis was carried out starting with one CFRP sheet layer at the bottom flange and more layers were added successively to study their effects on the structural performance of the beam. Beams strengthened with a lower number of layers of CFRP sheets failed due to the CFRP rupture at lower load levels. As the number of layers of CFRP sheets increased, the

mode of failure changed from CFRP rupture to plastic hinge formation at the top T-region, as shown in Figure 20. CFRP application at the bottom flange strengthened the bottom T-region and improved its stiffness. However, the un-strengthened top T-region, being subjected to higher flexural compressive stresses, failed in the observed manner.

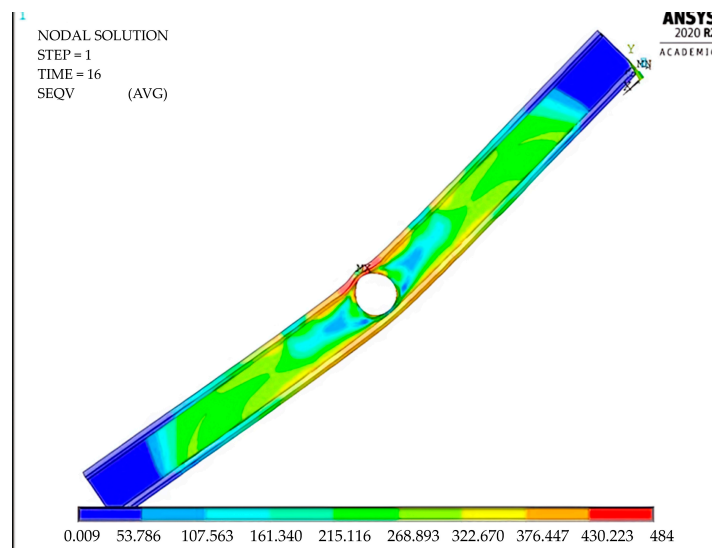


Figure 20. von Mises stress distribution at ultimate stage of strengthened D1H* beam using Scheme-I.

It was also observed that a plateau was reached and any additional layer beyond four layers had a negligible increase in the ultimate load of the beam. Therefore, Scheme-I was ineffective in strengthening SBWOs, since a plastic hinge was formed in the top T-region before the target load was reached for any additional layers of CFRP sheets.

The second strategy ‘Scheme-II’ was studied with the intent to address the limitation of the first scheme. Therefore, CFRP sheets were applied only to the bottom of the top flange, as shown in Figure 19b. The application of FRPs to the beam’s top flange offers several advantages, such as increasing the beam’s load capacity and stiffness, enhancing the top flange’s resistance to local buckling and providing tensile strength during reversed loading situations, like those encountered by beams in bridges [21]. The CFRP sheet layers were successively increased and the model was analyzed. Scheme-II was also found to be ineffective. The reason was that the bottom T-region around the opening yielded and the plastic hinge was formed, as shown in Figure 21. Moreover, the application of additional layers of CFRP sheets also did not play a role in achieving the target load, due to the prior bottom T-region failure.

In the third strengthening configuration, ‘Scheme-III’, CFRP sheets were applied to both the top and bottom flanges, as shown in Figure 19c. This strengthening scenario was adopted after the first two schemes proved ineffective in restoring the strength of the undamaged beam. The beam performed better than the previous cases, in terms of improving both the strength and stiffness, resulting in lower stress levels at both the top and bottom flanges at failure. However, localized stress concentrations were observed at the top and bottom T-regions (Figure 22) adjacent to the openings, prior to reaching the desired load level. This indicated that the strengthening of the flanges alone was not sufficient and needed to be extended to the web as well. Therefore, the fourth strengthening configuration, ‘Scheme-IV’, was considered next.

In ‘Scheme-IV’, CFRP sheets were applied to the bottom of both flanges, as well as on both sides of the web, as shown in Figure 19d. An equal number of layers of CFRP sheets were added successively. With six layers of CFRP sheets below the top and bottom flanges and on both sides of the web, this scheme was able to strengthen D1H* successfully, which sustained a load of 338 kN prior to failure (CFRP rupture). The stress distribution on the steel beam at failure for ‘Scheme-IV’ is shown in Figure 23. It can be seen from the figure

that the excessive stress was shifted away from the critical region near the opening toward the end of the CFRP sheet. This resulted in a higher load capacity and a more even stress distribution at the mid-span.

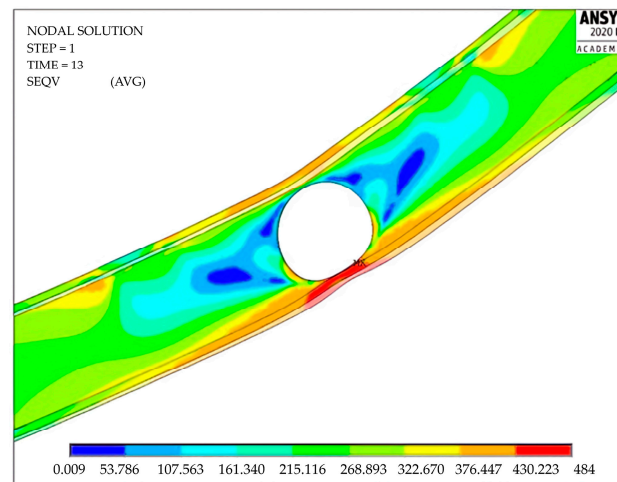


Figure 21. von Mises stress distribution at ultimate stage of strengthened D1H* beam using Scheme-II.

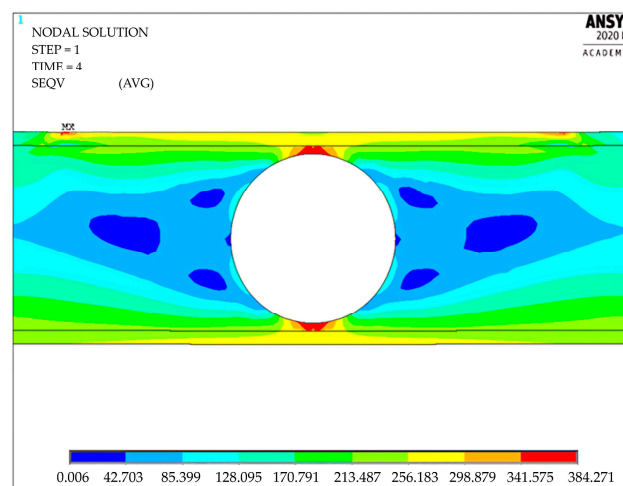


Figure 22. von Mises stress distribution of strengthened D1H* beam using Scheme-III.

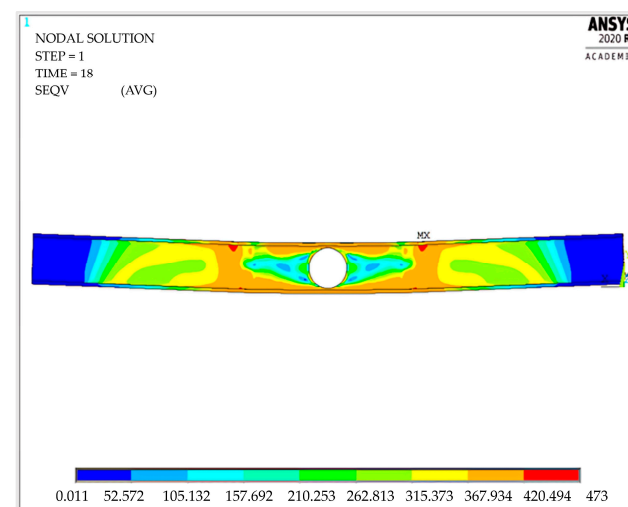


Figure 23. von Mises stress distribution at ultimate stage of strengthened D1H* beam using Scheme-IV.

As an alternative to ‘Scheme-IV’, another strengthening configuration, ‘Scheme-V’, was also studied. CFRP sheets were applied to the bottom of the top flange, to the top of the bottom flange, and on both sides of the web, as shown in Figure 19e. Like ‘Scheme-IV’, this strategy was also able to strengthen D1H* successfully with six CFRP sheet layers, which sustained a load of 332 kN prior to failure. The stress distribution on the steel beam at failure for ‘Scheme-V’ is shown in Figure 24.

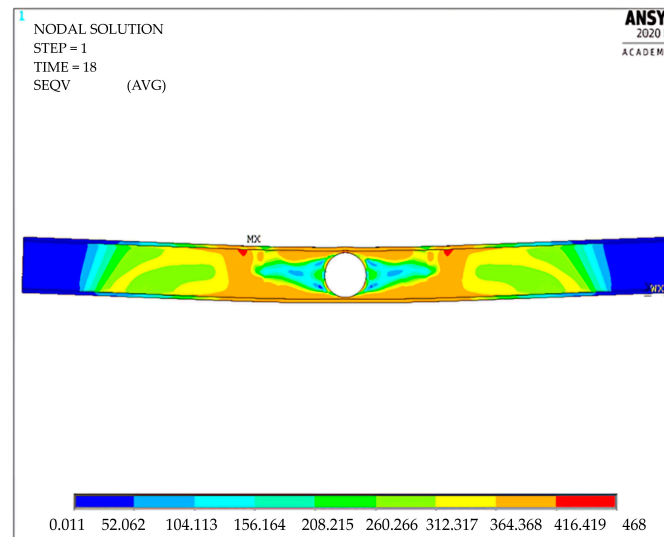


Figure 24. von Mises stress distribution at ultimate stage of strengthened D1H* beam using Scheme-V.

For the application of strengthening scheme-IV, it can be noted that the CFRP sheet must be cut into various pieces. To avoid such cuts, in the scheme-V strengthening configuration, continuous CFRP sheets were used on each side of the web and were extended to the total width of the flange as one piece. The difference in the failure load observed was negligible between the two schemes (338 kN and 332 kN). Additionally, the stress distribution in the CFRP sheets alone, as used in the ‘Scheme-V’ strengthening configuration, is shown in Figure 25, which indicates a lower stress level in the CFRP sheets towards the middle portion of the web. The reason behind such an observation was because the opening was in the bending-dominant low-shear region and the middle portion of the web in such a region would be subjected to a lower stress level. Thus, to economize ‘Scheme-V’, a final strengthening configuration of ‘Scheme-VI’ was proposed.

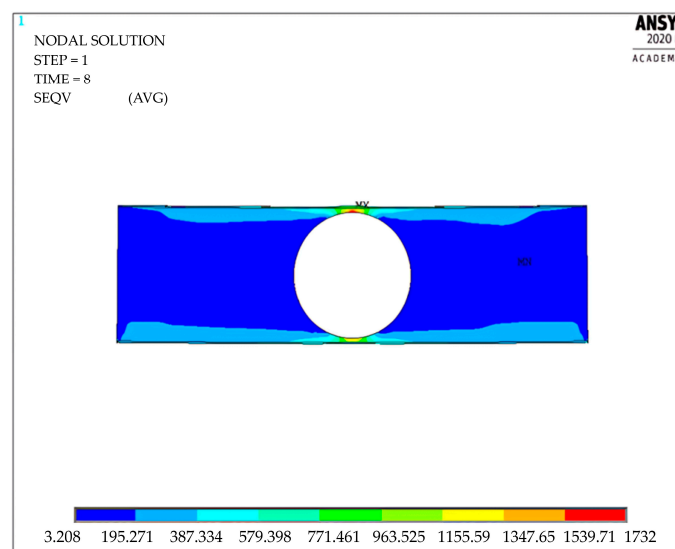


Figure 25. von Mises stress distribution in CFRP sheets (D1H* strengthened using scheme-V).

In ‘Scheme-VI’, CFRP sheets were applied on the bottom of the top flange, the top of the bottom flange, and on both sides of the web, covering only the top and bottom T-regions of the beam, as shown in Figure 19f. An equal number of layers of CFRP sheets was added successively. As anticipated, this scheme was also able to strengthen D1H* successfully with six CFRP sheet layers, which sustained a load of 331 kN prior to failure. The stress distribution of the strengthened beam at the ultimate stage for ‘Scheme-VI’ is shown in Figure 26, which closely resembles that of ‘Scheme-V’ (depicted in Figure 24), showing minimal differences.

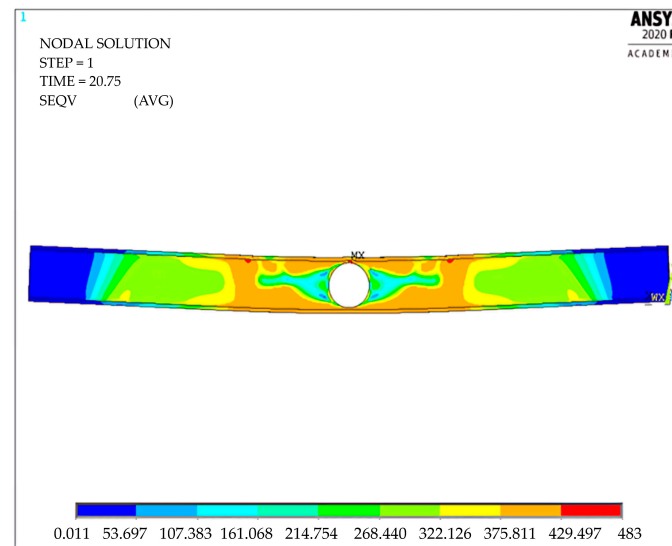


Figure 26. von Mises stress distribution at ultimate stage of strengthened D1H* beam using Scheme-VI.

In conclusion, three strengthening configurations, Scheme-IV, V, and VI, were able to strengthen D1H* to the desired level of strength. In all these strategies, a minimum of six CFRP sheet layers were needed. The load versus mid-span deflection diagram for D1H*, with these strengthening configurations, using six CFRP layers is shown in Figure 27. When compared with the control (CV-00) and damaged D1H* beam models, the strengthened beams had considerable enhancement in the stiffness in the inelastic regime after the yield point is reached. On the other hand, all strengthened models had an almost similar behavior with a slightly higher inelastic stiffness improvement, as the beam strengthened with scheme-IV. Based on the above observations, scheme-VI was found to be more efficient due to the lower material usage and greater cost-effectiveness.

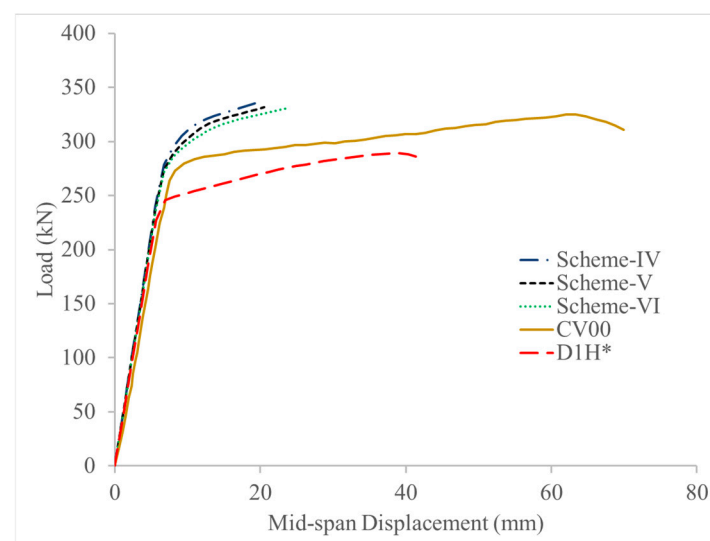


Figure 27. Load versus mid-span deflection diagram of D1H* beam with CFRP strengthening.

6. Conclusions

In the present study, finite element analysis was used to numerically investigate the efficacy of CFRP sheets on strengthening steel I-beams, damaged due to corrosion or cut-out web openings. FEA models were developed and validated against existing test specimens from the literature. Based on these validated models, a parametric investigation was carried out to examine the influence of various corrosion levels and cut-out web openings. Subsequently, CFRP sheets were applied to the bottom flanges of the corrosion-damaged steel I beams and the optimum number of CFRP layers required in restoring their capacities was investigated. Furthermore, six FRP strengthening configurations were proposed to restore the loss of the beam's strength, due to the damage induced by cut-out openings. Based on the parametric study results, the following conclusions were drawn:

- Due to the thinning of the bottom flange of the beam, both the yield and the ultimate load capacities of the beam were reduced. The reduction in the ultimate load followed a nearly perfect linear trend. For every 2.5% thickness loss of the bottom flange along 80% of the beam's span, the ultimate load was observed to reduce by roughly 1.5%.
- An adequate number of layers of CFRP sheets could restore both the yield and the ultimate load capacities of the beam subjected to corrosion damage to the level of the undamaged beam, while also increasing the overall beam stiffness. CFRP sheets, as a result, could be used as an alternative to CFRP plates or other conventional flexural strengthening techniques.
- The overall stiffness of the beams was observed to increase with the application of CFRP sheets. However, when a lower number of layers was used, the sheets ruptured before the desired level of load was reached, due to the overstressing of the thin sheets. Therefore, it is desirable to use a higher number of sheet layers for strengthening beams subjected to corrosion damage to delay sheet rupture, which could cause a sudden load drop in the beam.
- If the total area of the openings (sum of area of all openings) was kept constant, it was observed that beams with a greater number of circular web openings of smaller sizes had higher load capacities than those with a smaller number of larger web openings. Additionally, it is advisable to provide web openings in the bending predominant region of the beam's span.
- Three of the proposed strengthening configurations, which involved the application of CFRP sheets only to the bottom, the top, or both the bottom and the top flanges (Schemes-I, II, and III, respectively), were found to be ineffective. However, the remaining three strengthening configurations of Schemes-IV, V, and VI, which involved the application of CFRP sheets to both the flanges and the web, with a minimum of six layers of CFRP sheets, could restore the strength of the steel beam with circular web openings to the level of the one without openings. An additional number of CFRP sheet layers in these schemes would result in improvements in both the load-carrying capacity and stiffness of the beams.

The simplified FEA models developed in this study can be utilized for future research to highlight the influence of crucial parameters such as the mechanical properties of CFRPs and the types of fibers (i.e., Aramid, glass, and basalt) on the flexural and shear strengthening of damaged steel I-beams, particularly in steel bridges, where beams are subjected to fatigue loadings. Bearing that in mind, the findings of this research must be experimentally verified to ensure their practical applicability before being implemented in real-world scenarios.

Author Contributions: Conceptualization, A.P.; methodology, A.P. and P.K.S.; software, P.K.S. and M.A.; validation, P.K.S. and M.A.; investigation, P.K.S.; data curation, P.K.S.; writing—original draft preparation, P.K.S.; writing—review and editing, A.P. and M.A.; supervision, A.P.; project administration, A.P. All authors have read and agreed to the published version of the manuscript.

Funding: This research received no external funding.

Data Availability Statement: Data is contained within this article.

Conflicts of Interest: Author Mohannad Alhusban is employed by the company Crawford, Murphy & Tilly, Inc. The remaining authors declare that the research was conducted in the absence of any commercial or financial relationships that could be construed as a potential conflict of interest.

References

1. Tavakkolizadeh, M.; Saadatmanesh, H. Fatigue strength of steel girders strengthened with carbon fiber reinforced polymer patch. *J. Struct. Eng.* **2003**, *129*, 186–196. [CrossRef]
2. Ghafoori, E.; Motavalli, M. Normal, high and ultra-high modulus carbon fiber-reinforced polymer laminates for bonded and un-bonded strengthening of steel beams. *Mater. Des.* **2015**, *67*, 232–243. [CrossRef]
3. Kim, Y.J.; Harries, K.A. Fatigue behavior of damaged steel beams repaired with CFRP strips. *Eng. Struct.* **2011**, *33*, 1491–1502. [CrossRef]
4. Tafsirojjaman, T.; Fawzia, S.; Thambiratnam, D. Investigation on the behaviour of CFRP strengthened CHS members under monotonic loading through finite element modelling. *Structures* **2020**, *28*, 297–308. [CrossRef]
5. Tafsirojjaman, T.; Dogar, A.U.R.; Liu, Y.; Manalo, A.; Thambiratnam, D.P. Performance and design of Steel Structures Reinforced with FRP Composites: A state-of-the-art review. *Eng. Fail. Anal.* **2022**, *138*, 106371. [CrossRef]
6. Siwowski, T.W.; Siwowska, P. Experimental study on CFRP-strengthened steel beams. *Compos. Part B Eng.* **2018**, *149*, 12–21. [CrossRef]
7. Peiris, A.; Harik, I. Steel beam strengthening with UHM CFRP Strip Panels. *Eng. Struct.* **2021**, *226*, 111395. [CrossRef]
8. Bastani, A.; Das, S.; Kenno, S. Rehabilitation of thin walled steel beams using CFRP Fabric. *Thin-Walled Struct.* **2019**, *143*, 106215. [CrossRef]
9. Batuwitige, C.; Fawzia, S.; Thambiratnam, D.; Al-Mahaidi, R. Durability of CFRP strengthened steel plate double-strap joints in accelerated corrosion environments. *Compos. Struct.* **2017**, *160*, 1287–1298. [CrossRef]
10. Xu, S.; Li, H.; Wang, Y.; Wang, Y.; Wang, Y. Influence of corrosion on the bond behavior in CFRP-Steel Single Lap Joints. *Constr. Build. Mater.* **2020**, *236*, 117607. [CrossRef]
11. Li, H.; Xu, S.; Wang, Y.; Song, C. Deterioration of the bond behavior between CFRP and corroded steel in wet-dry cycling environment. *Compos. Struct.* **2021**, *272*, 114202. [CrossRef]
12. Morkhade, S.G.; Gupta, L.M. An experimental and parametric study on steel beams with web openings. *Int. J. Adv. Struct. Eng.* **2015**, *7*, 249–260. [CrossRef]
13. Morkhade, S.G.; Gupta, L.M. Experimental investigation for failure analysis of steel beams with web openings. *Steel Compos. Struct.* **2017**, *23*, 647–656. [CrossRef]
14. Morkhade, S.G.; Gupta, L.M. Ultimate load behaviour of steel beams with web openings. *Aust. J. Struct. Eng.* **2019**, *20*, 124–133. [CrossRef]
15. Morkhade, S.G.; Gupta, L.M. Critical study of steel beams with web openings. *Aust. J. Struct. Eng.* **2023**, *24*, 24–35. [CrossRef]
16. Abbas, J.L. Behaviour of steel I beams with web openings. *Civ. Eng. J.* **2023**, *9*, 596–617. [CrossRef]
17. Manoharan, A.C.; Tripathi, R.K. Analysis of steel beams with circular opening. *Int. J. Civ. Eng. Technol.* **2017**, *8*, 411–422.
18. Morkhade, S.G.; Kshirsagar, M.; Dange, R.; Patil, A. Analytical study of effect of web opening on flexural behaviour of hybrid beams. *Asian J. Civ. Eng.* **2019**, *20*, 537–547. [CrossRef]
19. Morkhade, S.G.; Lokhande, R.S.; Gund, U.D.; Divate, A.B.; Deosarkar, S.S.; Chavan, M.U. Structural behaviour of castellated steel beams with reinforced web openings. *Asian J. Civ. Eng.* **2020**, *21*, 1067–1078. [CrossRef]
20. Morkhade, S.G.; Jagtap, K.R.; Ghorpade, P.S.; Ahiwale, D.D.; Najm, H.M. Buckling performance evaluation of steel cellular beams strengthened with flange cover plate. *Asian J. Civ. Eng.* **2022**, *23*, 1277–1290. [CrossRef]
21. Altaee, M.J.; Cunningham, L.S.; Gillie, M. Experimental investigation of CFRP-strengthened steel beams with web openings. *J. Constr. Steel Res.* **2017**, *138*, 750–760. [CrossRef]
22. ANSYS®. *Academic Research Mechanical Release 20.2*; Help System; ANSYS, Inc.: Canonsburg, PA, USA, 2020; Available online: <http://www.ansys.com/> (accessed on 28 August 2023).
23. Lawson, R.M.; Hicks, S.J. *Design of Composite Beams with Large Web Openings: In Accordance with Eurocodes and the UK National Annexes*; Steel Construction Institute: Ascot, UK, 2011; ISBN 9781859421970.
24. Altaee, M.; Cunningham, L.; Gillie, M. Novel technique for strengthening steel beams with web penetrations. In Proceedings of the MACE PGR Conference, Manchester, UK, 22 March 2016.

Disclaimer/Publisher’s Note: The statements, opinions and data contained in all publications are solely those of the individual author(s) and contributor(s) and not of MDPI and/or the editor(s). MDPI and/or the editor(s) disclaim responsibility for any injury to people or property resulting from any ideas, methods, instructions or products referred to in the content.